Taylor & Francis
Taylor & Francis Group

BRIEF REPORT

🔓 OPEN ACCESS | Check for updates

Synthesis and antitumor activity of litseaone B analogues as tubulin polymerisation inhibitors

Wei Yang[a,d]*, Huining Peng[a,d]*, Yong Huang[c], Zhiyun Peng[b] and Guangcheng Wang[a] 🆔

[a]State Key Laboratory of Functions and Applications of Medicinal Plants, Guizhou Provincial Key Laboratory of Pharmaceutics, Guizhou Medical University, Guiyang, China; [b]Clinical Trails Center, The Affiliated Hospital of Guizhou Medical University, Guiyang, China; [c]Engineering Research Center for the Development and Application of Ethnic Medicine and TCM (Ministry of Education), Guizhou Medical University, Guiyang, China; [d]Teaching and Research Section of Natural Medicinal Chemistry, School of Pharmacy, Guizhou Medical University, Guiyang, China

ABSTRACT

A series of litseaone B analogues **4a~4p** were synthesised and antitumor activities of all compounds were screened. These compounds were designed by introducing different substituents on the B ring. Among these synthesised compounds, it was proved that **4k** showed excellent activity against A549, HepG2, and HCT-15 cell lines, the IC$_{50}$ values were 7.60 μM, 20.53 μM, and 4.59 μM, respectively. The results of tubulin polymerisation inhibition and immunofluorescence staining experiments displayed that **4k** could act on tubulin and inhibit the polymerisation of tubulin. Moreover, the wound healing assay showed that **4k** could inhibit the migration of A549 cells in a dose-dependent manner. Furthermore, the results of flow cytometry revealed that **4k** was capable of blocking the cell cycle in the G2/M phase, inducing a decrease in the mitochondrial membrane potential and ultimately leading to apoptosis in A549 cells. Importantly, the possible binding model was also performed by molecular docking.

Subject classification codes: short communication.

GRAPHICAL ABSTRACT
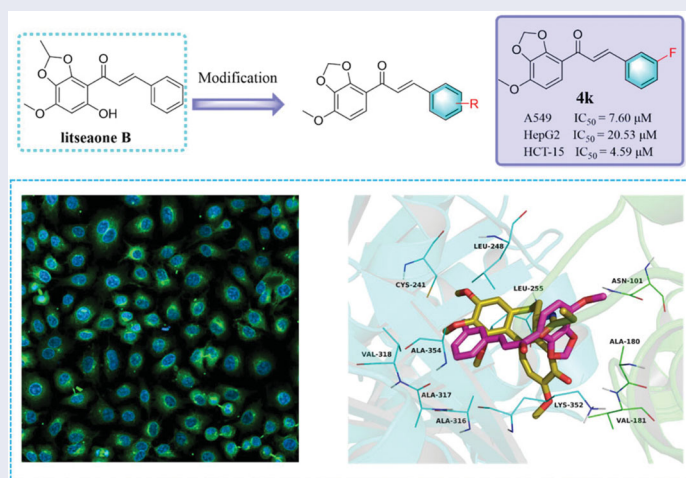
Introduction

Microtubules are essential cytoskeletal elements composed of α/β-tubulin heterodimers, which play important roles in various cellular processes, including determination and maintenance of cell shape, organisation of intracellular architecture, mitosis and cell division, secretion, intracellular transport and regulation of motility[1–3]. The disruption of microtubule function can block cell-division at the metaphase-anaphase transition and lead to the apoptosis of cancer cells[4]. Due to their essential role in mitotic spindle formation, microtubule has been considered as one of the most attractive targets for the design and development of anti-cancer agents[5–7].

Figure 1. Chemical structures of some natural products derived tubulin polymerisation inhibitors which are in clinical use or in clinical trials.
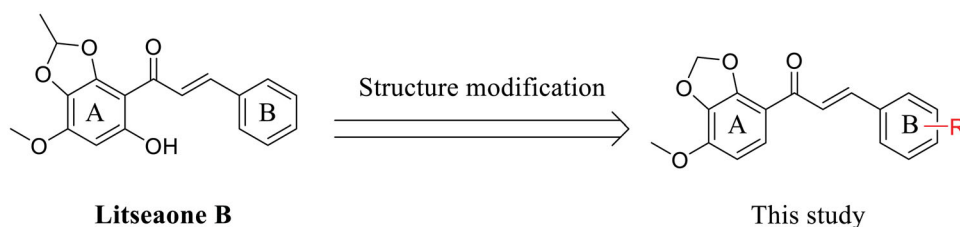
Figure 2. Rational design of litseaone B analogues.

Historically, natural products and their derivatives have been an important source of lead compounds for drug development and discovery[8]. Most of the currently approved drugs are natural products or synthetic natural products-derived compounds[8]. Hence, one of the strategies in drug design and development is to screen a large collection of natural products-based libraries and modify the structure of bioactive natural products[9–12]. Over the last few years, numerous structurally different natural products and their synthetic analogues had been identified as tubulin polymerisation inhibitors[13–15]. Among them, some of the compounds (synthetic or natural) had been used in clinical or preclinical trials, such as paclitaxel, docetaxel, vinblastine, vincristine, epothilone, combretastatin A-4P, and ombrabulin (Figure 1)[16].

Litsea is a genus of evergreen or deciduous trees or shrubs that grows in the mountains of China and other parts of Asia. Litsea plants exhibited various biological activities including anti-diarrheal, anti-HIV, anti-inflammation, antimicrobial, hypothermic, and antitumor[17,18]. In China, this genus is represented by 72 species, and some species are widely used in traditional Chinese medicine for the treatment of gastroenteralgia, edoema, and rheumatic arthritis[19]. Litseaone B, a natural chalcone, was for the first time isolated from the stem barks of *Litsea rubescens* and *Litsea pedunculata*[20]. It exhibited moderate cytotoxic activity with IC_{50} values of 21.5 μg/mL against the human liver carcinoma (HepG2) cell line. Furthermore, it also displayed more potent cytotoxic activities than cisplatin against myeloid leukaemia (HL-60) and epidermoid carcinoma (A431) cell lines with IC_{50} values of 10.2 and 13.9 μg/mL, respectively.

Based on the previous reports, one of the most widely proposed anticancer mechanisms of chalcones was to inhibit tubulin polymerisation by binding to the colchicine-binding site[21–24]. Considering the benefits above and in continuation of our interest in searching for novel tubulin polymerisation inhibitors[25–28], in the present study, we will describe the design, synthesis, and anticancer evaluation of a series of chalcones derivatives with litseaone B as a lead compound (Figure 2).

Materials and methods

Chemistry

Unless otherwise stated, all chemicals were purchased from commercial suppliers. Solvents and reagents were purified and dried as described in the literature. TLC was performed on 0.20 mm Silica Gel 60 F_{254} plates (Qingdao Ocean Chemical Factory, Shandong, China). Nuclear magnetic resonance spectra (NMR) were recorded on a Bruker spectrometer (400 MHz) with TMS as an external reference and reported in parts per million.

1–(7-Methoxybenzo[d][1,3] dioxol-4-yl)ethan-1-one (2)

To a solution of 1–(2,3-dihydroxy-4-methoxyphenyl)ethan-1-one **1** (15 mmol) in DMF (12 ml) was added K_2CO_3 (45 mmol) and CH_2Cl_2 (30 mmol), and the mixture was stirred at 90 °C for 6 h. After completion of the reaction, the reaction mixture was poured into ice-cold water and the product was extracted with ethyl acetate (100 ml × 3). The ethyl acetate solution with anhydrous Na_2SO_4 and the solvent was removed by distillation at reduced pressure.

The residue was purified by chromatography to afford product **2** (1.67 g, 57%) as a white solid.

General procedures for the synthesis of 4a-4o

To an ice-cold solution of 1–(7-methoxybenzo[d][1,3]dioxol-4-yl)ethan-1-one **2** (1 mmol) and commercially available aromatic aldehydes **3** (1 mmol) in CH_3OH (10 ml) was added 50% KOH aqueous solution (3 ml). The mixture was stirred in ice water for another 30 min, then at room temperature for 48 h. The mixture was poured on crushed ice and adjusted pH to 7 with 10% HCl. The precipitate was filtered, washed several times with water, and purified by recrystallization using EtOH to give desired products **4a**-**4o**.

(E)-3–(4-Chlorophenyl)-1–(7-methoxybenzo[d][1,3]dioxol-4-yl)prop-2-en-1-one (4a). Yellow solid (63%); ^1H NMR ($CDCl_3$, 400 MHz) δ: 3.96 (s, 3H), 6.14 (s, 2H), 6.62 (d, 1H, $J = 8.8$ Hz), 7.35 (d, 2H, $J = 8.8$ Hz), 7.54–7.56 (m, 3H), 7.62 (d, 1H, $J = 15.6$ Hz), 7.74 (d, 1H, $J = 15.6$ Hz); ^{13}C NMR ($CDCl_3$, 100 MHz) δ: 56.7, 102.2, 107.8, 115.6, 124.0, 125.2, 129.2, 129.8, 133.8, 135.4, 136.2, 142.2, 147.8, 149.0, 185.7; HRMS (ESI) calcd for $[M + H]^+$ $C_{17}H_{14}ClO_4^+$: 317.05751 found 317.05569.

(E)-1–(7-Methoxybenzo[d][1,3] dioxol-4-yl)-3–(4-methoxyphenyl)-prop-2-en-1-one (4 b). Yellow solid (71%); ^1H NMR ($CDCl_3$, 400 MHz) δ: 3.84 (s, 3H), 3.95 (s, 3H), 6.13 (s, 2H), 6.61 (d, 1H, $J = 8.8$ Hz), 6.90 (d, 2H, $J = 8.8$ Hz), 7.53–7.59 (m, 4H), 7.78 (d, 1H, $J = 15.6$ Hz); ^{13}C NMR ($CDCl_3$, 100 MHz) δ: 55.5, 56.7, 102.1, 107.6, 114.4, 116.0, 122.4, 123.9, 128.0, 130.4, 135.4, 143.6, 147.5, 148.9, 161.6, 161.6, 186.0; HRMS (ESI) calcd for $[M + H]^+$ $C_{18}H_{17}O_5^+$: 313.10705 found 313.10519.

(E)-3–(4-(Diethylamino)phenyl)-1–(7-methoxybenzo[d][1,3]dioxol-4-yl) prop-2-en-1-one (4c). Yellow solid (19%); ^1H NMR ($CDCl_3$, 400 MHz) δ: 1.19 (t, 3H, $J = 6.8$ Hz), 3.37 (q, 2H, $J = 6.8$ Hz), 3.95 (s, 3H), 6.11 (s, 2H), 6.60 (d, 1H, $J = 8.8$ Hz), 6.64 (d, 2H, $J = 7.2$ Hz), 7.43 (d, 1H, $J = 15.6$ Hz), 7.50 (d, 2H, $J = 8.8$ Hz), 7.53 (d, 1H, $J = 8.8$ Hz), 7.78 (d, 1H, $J = 15.6$ Hz); ^{13}C NMR ($CDCl_3$, 100 MHz) δ: 12.7, 44.6, 56.6, 101.9, 107.6, 111.4, 116.6, 119.1, 122.3, 123.8, 130.8, 144.8, 147.1, 148.6, 149.6, 186.0; HRMS (ESI) calcd for $[M + H]^+$ $C_{21}H_{24}NO_4^+$: 354.16998 found 354.16748.

(E)-3–(4-(Dimethylamino)phenyl)-1–(7-methoxybenzo[d][1,3]dioxol-4-yl) prop-2-en-1-one (4d). Yellow solid (50%); ^1H NMR ($CDCl_3$, 400 MHz) δ: 3.02 (s, 6H), 3.95 (s, 3H), 6.13 (s, 2H), 6.98 (d, 1H, $J = 8.8$ Hz), 6.67 (d, 2H, $J = 8.8$ Hz), 7.52 (d, 2H, $J = 8.8$ Hz), 7.53 (d, 1H, $J = 8.8$ Hz), 7.45 (d, 1H, $J = 15.6$ Hz), 7.79 (d, 1H, $J = 15.6$ Hz); ^{13}C NMR ($CDCl_3$, 100 MHz) δ: 40.2, 56.6, 102.0, 107.6, 111.9, 116.5, 119.7, 123.8, 130.5, 135.4, 144.7, 147.2, 148.7, 152.0, 186.0; HRMS (ESI) calcd for $[M + H]^+$ $C_{19}H_{20}NO_4^+$: 326.13868 found 326.13663.

(E)-1–(7-Methoxybenzo[d][1,3]dioxol-4-yl)-3–(3,4,5-trimethoxyphenyl) prop-2-en-1-one (4e). Yellow solid (71%); ^1H NMR ($CDCl_3$, 400 MHz) δ: 3.88 (s, 3H), 3.90 (s, 6H), 3.97 (s, 3H), 6.13 (s, 2H), 6.62 (d, 1H, $J = 8.8$ Hz), 6.85 (s, 2H), 7.49–7.55 (m, 2H), 7.71 (d, 1H, $J = 15.6$ Hz); ^{13}C NMR ($CDCl_3$, 100 MHz) δ: 56.3, 56.7, 61.1, 102.1, 106.0, 107.8, 123.9, 130.8, 135.4, 140.5, 143.8, 147.6, 148.9, 153.5, 153.5, 185.9; HRMS (ESI) calcd for $[M + H]^+$ $C_{20}H_{21}O_7^+$: 373.12818 found 373.12534.

(E)-1–(7-Methoxybenzo[d][1,3]dioxol-4-yl)-3-phenylprop-2-en-1-one (4f). Yellow solid (73%); ^1H NMR ($CDCl_3$, 400 MHz) δ: 3.96 (s, 3H), 6.13 (s, 2H), 6.12 (d, 1H, $J = 8.8$ Hz), 7.38–7.41 (m, 3H), 7.55 (d, 1H, $J = 8.8$ Hz), 7.62–7.64 (m, 2H), 7.65 (d, 1H, $J = 15.6$ Hz), 7.80 (d, 1H, $J = 8.8$ Hz); ^{13}C NMR ($CDCl_3$, 100 MHz) δ: 56.7, 102.1, 107.8, 115.8, 123.9, 124.7, 128.6, 128.9, 130.4, 135.3, 135.4, 143.7, 147.6, 149.0, 186.0; HRMS (ESI) calcd for $[M + H]^+$ $C_{17}H_{15}O_4^+$: 283.09649 found 283.09512.

(E)-3–(2-Fluorophenyl)-1–(7-methoxybenzo[d][1,3]dioxol-4-yl)prop-2-en-1-one (4 g). Yellow solid (53%); ^1H NMR ($CDCl_3$, 400 MHz) δ: 3.96 (s, 3H), 6.13 (s, 2H), 6.61 (d, 1H, $J = 8.8$ Hz), 7.10 (t, 1H, $J = 8.8$ Hz), 7.17 (d, 1H, $J = 8.0$ Hz), 7.32–7.38 (m, 1H), 7.54 (d, 1H, $J = 8.8$ Hz), 7.64 (dt, 1H, $J = 8.0$ Hz, 1.2 Hz), 7.39 (d, 1H, $J = 15.6$ Hz), 7.91 (d, 1H, $J = 15.6$ Hz); ^{13}C NMR ($CDCl_3$, 100 MHz) δ: 56.7, 102.2, 107.7, 115.6, 116.2 (d, 1 C, $J = 21.8$ Hz), 123.3 (d, 1 C, $J = 11.7$ Hz), 124.0, 124.5 (d, 1 C, $J = 3.5$ Hz), 127.0 (d, 1 C, $J = 6.6$ Hz), 129.6, 129.7, 131.7 (d, 1 C, $J = 8.7$ Hz), 135.4, 136.2, 147.1, 149.1, 160.5 (d, 1 C, $J = 253.2$ Hz), 186.0; HRMS (ESI) calcd for $[M + H]^+$ $C_{17}H_{14}FO_4^+$: 301.08706 found 301.08560.

(E)-1–(7-Methoxybenzo[d][1,3]dioxol-4-yl)-3-(naphthalen-1-yl)prop-2-en-1-one (4 h). Yellow solid (76%); ^1H NMR ($CDCl_3$, 400 MHz) δ: 3.97 (s, 3H), 6.14 (s, 2H), 6.64 (d, 1H, $J = 8.8$ Hz), 7.49–7.62 (m, 4H), 7.74 (d, 1H, $J = 15.6$ Hz), 7.86–7.91 (m, 3H), 8.27 (d, 1H, $J = 8.8$ Hz), 8.65 (d, 1H, $J = 15.6$ Hz); ^{13}C NMR ($CDCl_3$, 100 MHz) δ: 56.7, 102.2, 107.8, 123.7, 124.0, 125.3, 126.3, 127.0, 128.8, 130.7, 131.9, 132.7, 133.8, 135.4, 140.6, 147.7, 149.1, 185.9; HRMS (ESI) calcd for $[M + H]^+$ $C_{21}H_{17}O_4^+$: 333.11214 found 333.11999.

(E)-3–(4-Bromophenyl)-1–(7-methoxybenzo[d][1,3]dioxol-4-yl)prop-2-en-1-one (4i). Yellow solid (77%); ^1H NMR ($CDCl_3$, 400 MHz) δ: 3.94 (s, 3H), 6.12 (s, 2H), 6.59 (d, 1H, $J = 8.8$ Hz), 7.44 (d, 2H, $J = 8.8$ Hz), 7.49 (d, 2H, $J = 8.8$ Hz), 7.52 (d, 1H, $J = 8.8$ Hz), 7.61 (d, 1H, $J = 15.6$ Hz), 7.70 (d, 1H, $J = 15.6$ Hz); ^{13}C NMR ($CDCl_3$, 100 MHz) δ: 56.7, 102.2, 107.8, 115.5, 123.9, 124.6, 125.2, 130.0, 132.2, 134.1, 135.4, 142.2, 147.7, 149.0, 185.6; HRMS (ESI) calcd for $[M + H]^+$ $C_{17}H_{14}BrO_4^+$: 361.00700 found 361.00485.

(E)-3–(4-Fluorophenyl)-1–(7-methoxybenzo[d][1,3]dioxol-4-yl)prop-2-en-1-one (4j). Yellow solid (72%); ^1H NMR ($CDCl_3$, 400 MHz) δ: 3.95 (s, 3H), 6.13 (s, 2H), 6.61 (d, 1H, $J = 8.8$ Hz), 7.07 (t, 2H, $J = 8.8$ Hz), 7.53–7.62 (m, 4H), 7.75 (d, 1H, $J = 15.6$ Hz); ^{13}C NMR ($CDCl_3$, 100 MHz) δ: 56.7, 102.2, 107.7, 115.6, 116.0 (d, 2 C, $J = 21.8$ Hz), 123.9, 124.4 (d, 1 C, $J = 1.5$ Hz), 130.4 (d, 1 C, $J = 8.5$ Hz), 131.5, 131.5, 135.4, 142.4, 147.7, 149.0, 162.8 (d, 1 C, $J = 250.2$ Hz), 185.7; HRMS (ESI) calcd for $[M + H]^+$ $C_{17}H_{14}FO_4^+$: 301.08706 found 301.08548.

(E)-3–(3-Fluorophenyl)-1–(7-methoxybenzo[d][1,3]dioxol-4-yl)prop-2-en-1-one (4k). Yellow solid (63%); ^1H NMR ($CDCl_3$, 400 MHz) δ: 3.97 (s, 3H), 6.15 (s, 2H), 6.63 (d, 1H, $J = 8.8$ Hz), 7.06–7.11 (m, 1H), 7.32–7.38 (m, 3H), 7.55 (d, 1H, $J = 8.8$ Hz), 7.64 (d, 1H, $J = 15.6$ Hz), 7.75 (d, 1H, $J = 15.6$ Hz); ^{13}C NMR ($CDCl_3$, 100 MHz) δ: 56.7, 102.2, 107.8, 114.4 (d, 1 C, $J = 21.7$ Hz), 117.1 (d, 1 C, $J = 21.2$ Hz), 124.0, 124.8, 125.9, 130.5 (d, 1 C, $J = 8.4$ Hz), 135.4, 137.5 (d, 1 C, $J = 7.5$ Hz), 142.2, 147.8, 149.1, 161.9 (d, 1 C, $J = 245.0$ Hz); HRMS (ESI) calcd for $[M + H]^+$ $C_{17}H_{14}FO_4^+$: 301.08706 found 301.08548.

(E)-1–(7-Methoxybenzo[d][1,3]dioxol-4-yl)-3–(2,3,4-trimethoxyphenyl) prop-2-en-1-one (4 l). Yellow solid (82%); ^1H NMR ($CDCl_3$, 400 MHz) δ: 3.88 (s, 3H), 3.90 (s, 3H), 3.93 (s, 3H), 3.96 (s, 3H), 6.12 (s, 2H), 6.62 (d, 1H, $J = 8.8$ Hz), 6.70 (d, 1H, $J = 8.8$ Hz), 7.37 (d, 1H, $J = 8.8$ Hz), 7.55 (d, 1H, $J = 8.8$ Hz), 7.66 (d, 1H, $J = 15.6$ Hz), 7.99 (d,

1H, $J = 15.6$ Hz); ^{13}C NMR (CDCl$_3$, 100 MHz) δ: 56.2, 56.6, 61.0, 61.5, 102.1, 107.6, 107.6, 116.1, 122.4, 124.0, 124.1, 135.3, 139.0, 142.5, 147.4, 148.9, 153.9, 155.7, 186.3; HRMS (ESI) calcd for [M + H]$^+$ C$_{20}$H$_{21}$O$_7^+$: 373.12818 found 373.12552.

(E)-1–(7-Methoxybenzo[d][1,3]dioxol-4-yl)-3-(naphthalen-2-yl)prop-2-en-1-one (4 m). Yellow solid (87%); ^{1}H NMR (CDCl$_3$, 400 MHz) δ: 3.97 (s, 3H), 6.17 (s, 2H), 6.63 (d, 1H, $J = 8.8$ Hz), 7.50–7.52 (m, 2H), 7.58 (d, 1H, $J = 8.8$ Hz), 7.56–7.89 (m, 5H), 7.97 (d, 2H, $J = 15.6$ Hz); ^{13}C NMR (CDCl$_3$, 100 MHz) δ: 56.7, 102.2, 107.7, 115.8, 123.9, 124.0, 124.8, 126.8, 127.9, 128.7, 128.7, 130.8, 132.8, 133.5, 134.4, 135.4, 143.8, 147.7, 149.0, 185.9; HRMS (ESI) calcd for [M + H]$^+$ C$_{21}$H$_{17}$O$_4^+$: 333.11214 found 333.11044.

(E)-3–(3-Chlorophenyl)-1–(7-methoxybenzo[d][1,3]dioxol-4-yl)prop-2-en-1-one (4n). Yellow solid (63%); ^{1}H NMR (CDCl$_3$, 400 MHz) δ: 3.97 (s, 3H), 6.15 (s, 2H), 6.62 (d, 1H, $J = 8.8$ Hz), 7.30–7.36 (m, 2H), 7.47–7.48 (m, 1H), 7.54 (d, 1H, $J = 8.8$ Hz), 7.60 (s, 1H), 7.63 (d, 1H, $J = 15.6$ Hz), 7.72 (d, 1H, $J = 15.6$ Hz); ^{13}C NMR (CDCl$_3$, 100 MHz) δ: 56.7, 102.2, 107.9, 115.5, 124.0, 125.9, 127.0, 128.0, 130.2, 134.9, 135.4, 137.1, 141.9, 147.8, 149.1, 185.6; HRMS (ESI) calcd for [M + H]$^+$ C$_{17}$H$_{14}$ClO$_4^+$: 317.05751 found 317.05566.

(E)-3–(4-Methoxy-3-(methoxymethoxy)phenyl)-1–(7-methoxybenzo[d] [1,3]dioxol-4-yl)prop-2-en-1-one (4o). Yellow solid (56%); ^{1}H NMR (CDCl$_3$, 400 MHz) δ: 3.53 (s, 3H), 3.91 (s, 3H), 3.95 (s, 3H), 5.26 (s, 2H), 6.12 (s, 2H), 6.61 (d, 1H, $J = 8.8$ Hz), 6.89 (d, 1H, $J = 8.8$ Hz), 7.27 (dd, 1H, $J = 8.8$ Hz, 1.6 Hz), 7.45 (d, 1H, $J = 1.6$ Hz), 7.50 (d, 1H, $J = 15.6$ Hz), 7.52 (d, 1H, $J = 8.8$ Hz), 7.73 (d, 1H, $J = 15.6$ Hz); ^{13}C NMR (CDCl$_3$, 100 MHz) δ: 56.1, 56.4, 56.6, 95.7, 102.1, 107.6, 111.6, 116.0, 122.9, 123.9, 124.3, 128.4, 135.4, 143.6, 146.7, 147.5, 148.9, 151.9, 186.0; HRMS (ESI) calcd for [M + H]$^+$ C$_{20}$H$_{21}$O$_7^+$: 373.12818 found 373.12543.

(E)-3–(3-Hydroxy-4-methoxyphenyl)-1–(7-methoxybenzo[d][1,3]-dioxol-4-yl)prop-2-en-1-one (4p). To a solution of compound **4o** (1.0 mmol) in EtOH (20 ml) was added concentrated HCl (1 ml) and stirred at 80 °C for 1 h. After completion of the reaction, the solvent was evaporated under reduced pressure and the residue was purified by chromatography to obtain compound **4p**. Yellow solid (84%); ^{1}H NMR (CDCl$_3$, 400 MHz) δ: 3.92 (s, 3H), 3.96 (s, 3H), 5.72 (s, 1H), 6.13 (s, 2H), 6.61 (d, 1H, $J = 8.8$ Hz), 6.84 (d, 1H, $J = 8.8$ Hz), 7.09 (d, 1H, $J = 8.8$ Hz, 2.0 Hz), 7.29 (d, 1H, $J = 2.0$ Hz), 7.52 (d, 1H, $J = 15.2$ Hz), 7.54 (d, 1H, $J = 8.8$ Hz), 7.73 (d, 1H, $J = 15.2$ Hz); ^{13}C NMR (CDCl$_3$, 100 MHz) δ: 56.1, 56.7, 102.1, 107.6, 110.6, 112.8, 115.9, 122.9, 123.2, 123.9, 128.9, 135.4, 143.7, 145.9, 147.5, 148.8, 148.9, 185.9; HRMS (ESI) calcd for [M + H]$^+$ C$_{18}$H$_{17}$O$_6^+$: 329.10196 found 329.09985.

Biological section

Antiproliferative activity
A549, HepG2, and HCT-15 cell lines were inoculated in 96-well plates (1×10^3 ~3×10^3 cells/well) and incubated at 37 °C for 24 h. After that, cells were treated with various concentrations of synthesised compounds for 72 h. Then 15 μL MTT (5 mg/mL) was added to each well of 96-well plates and incubated for 1~4 h. Later, discarded the solution in the 96-well plates and added DMSO solution at a volume of 150 μL/well, shaking for 1 0~20 min, and the multifunction microplate reader determines the absorbance of each well at a wavelength of 490 nm. The IC$_{50}$ values were calculated by GraphPad Prism 8. All experiments were repeated three times.

Inhibitory effect of 4k on intracellular tubulin polymerisation
Tubulin protein was mixed with various concentrations of compound **4k** in PEM buffer, which consists of 100 mM PIPES, 1 mM MgCl$_2$, and 1 mM EGTA, containing 5% glycerol and 1 mM GTP. The process of tubulin polymerisation was monitored by light scattering at 340 nm using a SPECTRA MAX 190 (Molecular Device) spectrophotometer at 37 °C. The measured plateau absorbance values are used for subsequent calculations.

Immunofluorescence staining
A549 cells ($1 \times 10^5 \sim 4 \times 10^5$ cells/well) were seeded in confocal dedicated petri dishes (volume of 500 μL/well) and cultured for 24 h. Then added **4k** with concentrations of 10, 15, and 20 μM, and the control group was added the same volume of complete medium. Next, A549 cells were fixed with 3.7% paraformaldehyde for 30 min and stained by α-tubulin (Alpha Tubulin Recombinant antibody, cat. 80762–1-RR) overnight. Lastly, A549 cells were stained with Hoechst 33342 (20 μg/mL). A549 cells were imaged by ZEISS LSM900 Airyscan laser scanning confocal microscope.

Wound healing assay
A549 cells were seeded in 6-well plates at a density to ensure that the cells could overgrow overnight. Then, created three or more scratches by scraping vertically with a 10 μL pipette tip in a well, and washed all wells with PBS at least three times. Afterward, A549 cells were incubated with different concentrations of **4k**. After incubating for 24 h, images were photographed by inverted microscope and the wound healing rate was analysed by Image J.

Cell apoptosis analysis
A549 cells (1×10^5 cells/well) were seeded in 6-well plates and cultured for 24 h. Then treated with different concentrations of **4k** for 72 h, collected cells with 5 ml centrifuge tubes, and washed them twice. After that, resuspend cells with 1 ml PBS, then centrifuged (1500r/min, 10 min). Afterward, added 100 μL of apoptosis staining solution (5 μL Annexin V, 5 μL PI, and 1 × binding Buffer) and stained for 15 min at room temperature without light. At last, 500 μL 1× binding buffer was added to the suspension evenly, and samples were analysed by flow cytometric detection.

The analysis of mitochondrial membrane potential
A549 cells (1×10^5/well) were seeded in 6-well plates, after culturing for 24 h, different concentrations of **4k** were added, and the control group was only dealt with the same volume of complete medium. After exposing the A549 cells to different concentrations of compound **4k** for 72 h, collected the cells and washed them twice with PBS. Then stained with 300 μL JC-1 staining solution at 37 °C for 20 min. After that, centrifuged and added 500 μL of JC-1 staining buffer to resuspend, centrifuged again. Then added 1 ml of PBS to resuspend the cells and detected by flow cytometry.

Cell cycle analysis
A549 cells were treated with different concentrations of **4k** for 72 h. Then, digested, centrifuged (1500 r/min, 10 min), and discarded the supernatant. Collected cells and fixed cells with pre-chilled 70% ethanol in a −20 °C refrigerator overnight. Cells were washed with PBS and resuspended with RNase A solution with a volume of 100 μL in a 37 °C water bath for 30 min. Then stained with 400 μL of PI staining solution and incubated at 4 °C for 30 min without light. Finally, all samples were tested by flow cytometry at 580 nm.
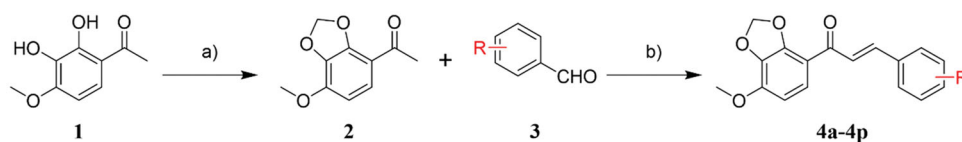
Scheme 1. (a) CH_2Cl_2, K_2CO_3, DMF, 90 °C, 6 h; (b) KOH (a.q.), CH_3OH, 0 °C, 30 min → rt, 48 h; (c) **4p**: **4o**, HCl(c), EtOH, 80 °C, 1 h.

Table 1. Evaluation of anti-tumour proliferative activity of synthesised compounds.

Compounds	R	IC$_{50}$±SD (μM)[a]		
		A549	HepG2	HCT-15
4a	4-Cl	7.57 ± 0.52	33.27 ± 1.35	9.98 ± 0.05
4b	4-OCH$_3$	>50	>50	19.61 ± 0.70
4c	4-diethylamino	>50	>50	>50
4d	4-dimethylamino	>50	>50	48.74 ± 1.86
4e	3,4,5-trimethoxy	>50	>50	2.36 ± 0.96
4f	H	8.82 ± 0.23	>50	12.90 ± 0.52
4g	2-F	20.03 ± 2.21	20.5 ± 1.84	>50
4h	1-naphthyl	24.33 ± 0.56	43.72 ± 2.27	5.37 ± 0.12
4i	4-Br	13.70 ± 0.65	14.96 ± 0.25	10.58 ± 0.49
4j	4-F	9.54 ± 0.93	>50	>50
4k	3-F	7.60 ± 0.18	20.53 ± 0.59	4.59 ± 0.14
4l	2,3,4-trimethoxy	19.20 ± 0.71	31.84 ± 0.31	8.96 ± 0.37
4m	2-naphthyl	35.60 ± 1.75	>50	>50
4n	3-Cl	15.47 ± 0.26	13.67 ± 1.43	14.95 ± 0.46
4o	3-methoxymethoxy, 4-OCH$_3$	13.69 ± 0.45	19.02 ± 1.67	11.95 ± 0.40
4p	3-OH, 4-OCH$_3$	8.91 ± 0.34	14.13 ± 0.24	8.89 ± 0.05
Cisplatin	–	5.49 ± 0.14-	26.82 ± 1.81	1.98 ± 0.06
Paclitaxel	–	8.03 ± 0.78	10.53 ± 0.63	3.28 ± 0.28
Colchicine	–	2.74 ± 1.09	5.75 ± 0.14	1.59 ± 0.05

[a]Data are presented as mean ± SD of at least three independent experiments.

Molecular docking study

Molecular docking study was performed by using Autodock vina 1.1.2. The 3 D structure of tubulin was downloaded from the website of the protein data bank (www.rcsb.org), while the 3 D structure of 4k was drawn in ChemBio3D software. Besides, the ligand-protein complex was imaged using PyMoL 1.7.6 software (www.pymol.org), and the value of exhaustiveness was set to 16. For Vina docking.

Results and discussions

Chemistry

The synthetic pathway to achieve the title compounds **4a-4p** was shown in Scheme 1. 1–(7-Methoxybenzo[d][1,3]dioxol-4-yl)ethan-1-one **2** was prepared by condensation of commercial available 1–(2,3-dihydroxy-4-methoxyphenyl)ethan-1-one **1** with CH_2Cl_2 in the presence of K_2CO_3 as a base at 90 °C. The title compounds **4a-4o** were prepared by Claisen-Schmidt condensation. To an ice-cold solution of **2** and commercially available aromatic aldehydes **3** in CH_3OH was added 50% KOH aqueous solution. The mixture was stirred in ice water for another 30 min, then at room temperature for 48 h. After completion of the reaction, the mixture was treated with ice-cold water and adjusted pH to 7 using 10% HCl. The precipitate was collected by filtration and recrystallization from ethanol to give the desired compounds **4a-4o** in moderate to high yields. Removal of the MOM group of the compound **4o**

under the acid condition to obtain compound **4p** in high yield. The structures of these compounds were elucidated by ^{1}H NMR, ^{13}C NMR, and HRMS (Supplemental Material, Figure S1-S48).

Biological evaluation

Antiproliferative activity

All synthesised compounds (**4a∼4p**) were assayed via the MTT method to evaluate the potential ability of these compounds against three common cancer cell lines including HepG2 (liver cancer cell), A549 (lung cancer cell), and HCT-15 (colon cancer cell) (Table 1). All cancer cell lines were treated with compounds at different concentrations (3.125 μM, 6.25 μM, 12.5 μM, 25 μM, and 50 μM) and all results were analysed after 72 h. Moreover, antiproliferative activity was calculated based on the IC$_{50}$ values shown in Table 1. The cisplatin, paclitaxel, and colchicine were tested as positive compounds. The results displayed that most of the target compounds showed significant inhibition against A549 cells and HCT-15 cells, while showed moderate antiproliferative activity on HepG2 cells. Especially, the compound with the substituent of 3-F (**4k**) had excellent antiproliferative activity on three cancer cells with IC$_{50}$ values ranging from 4.59 μM to 20.53 μM. However, with the position of the F atom changed, the antiproliferative activity on tumour cells would be changed as well. For example, when compared with compound **4k**, the inhibition of tumour cell proliferation activity will be attenuated with the fluorine atom changed
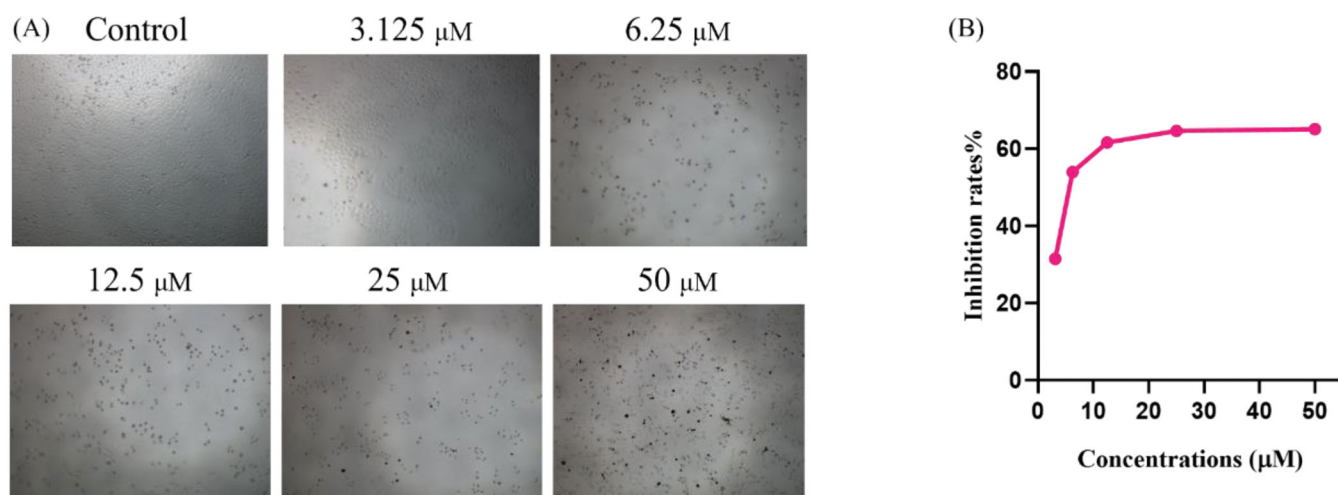
Figure 3. (A) Images of morphologies of A549 cells treated with different concentrations of **4k** for 72 h. (B) The line chart of inhibition rates of A549 cells treated with different concentrations of **4k** for 72 h.
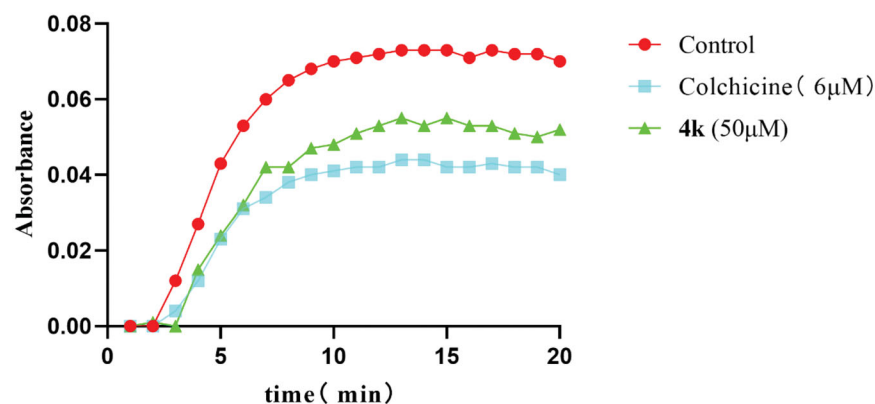
Figure 4. Effect of Colchicine (6 μM) and **4k** (50 μM) on tubulin polymerisation.
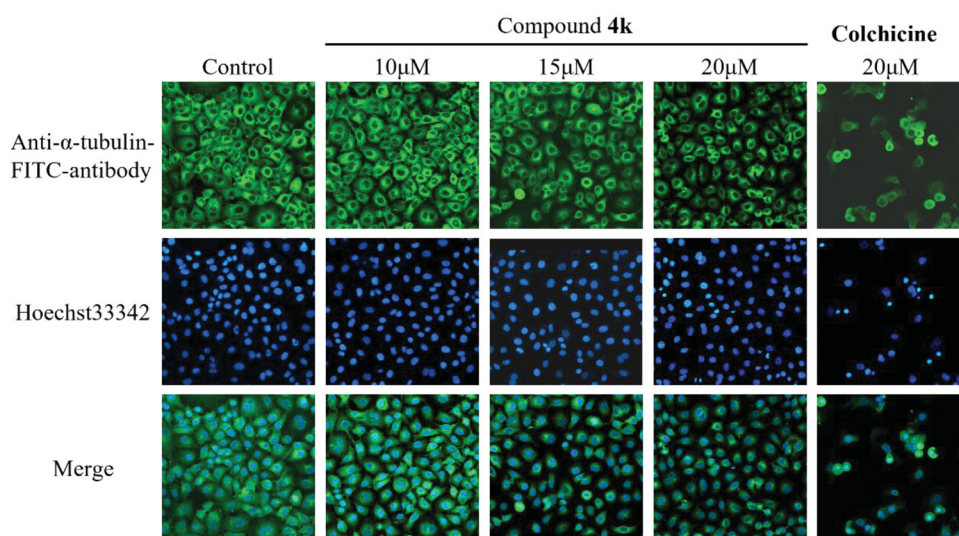
Figure 5. Effect of **4k** on tubulin in A549 cells. The A549 cells were treated with colchicine (20 μM) and different concentrations of **4k** for 24 h, and the distribution of tubulin in the cells was observed by laser scanning confocal microscopy.

into position 2 or position 4. Besides, when the substituent was changed into 4-Cl (**4a**), the compound also demonstrated potent cell cytotoxicity on three cell lines with IC$_{50}$ values between 7.57 μM and 33.27 μM. Furthermore, the presence of diethylamino (**4c**) and dimethylamino (**4d**) showed poor activity to inactive on

all cell lines. To sum up, among these cancer cells, **4k** was most sensitive to HCT-15 cells, followed by A549 cells. But in our actual work, it was found that A549 cells had a stronger migration ability than HCT-15 cells, so A549 cells were selected for follow-up mechanism research. The morphologies and inhibition rates of A549

(A)

(B)
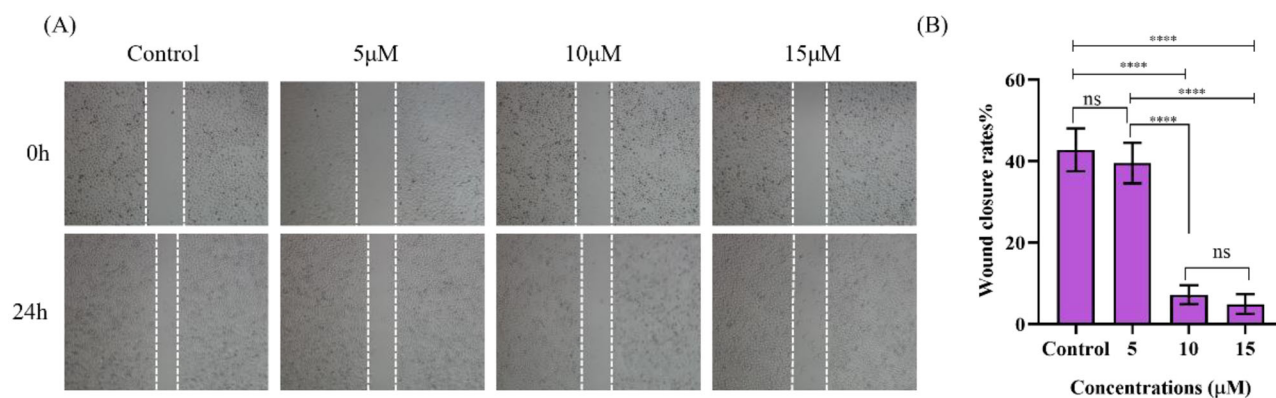
Figure 6. Compound **4k** inhibited the migration of A549 in the wound healing (A and B). (A) Images of wound area in a scratch assay of A549 cells treated with different concentrations of **4k** after 24 h, (B) The image of wound closure rates of A549 cells treated with different concentrations of **4k** after 24 h. Data in figure B are means ± SD of three independent replicates, ns*$p < 0.05$, **$p < 0.01$, ***$p < 0.001$, ****$p < 0.0001$, ns: no significance, one-way ANOVA.

(A)

(B)
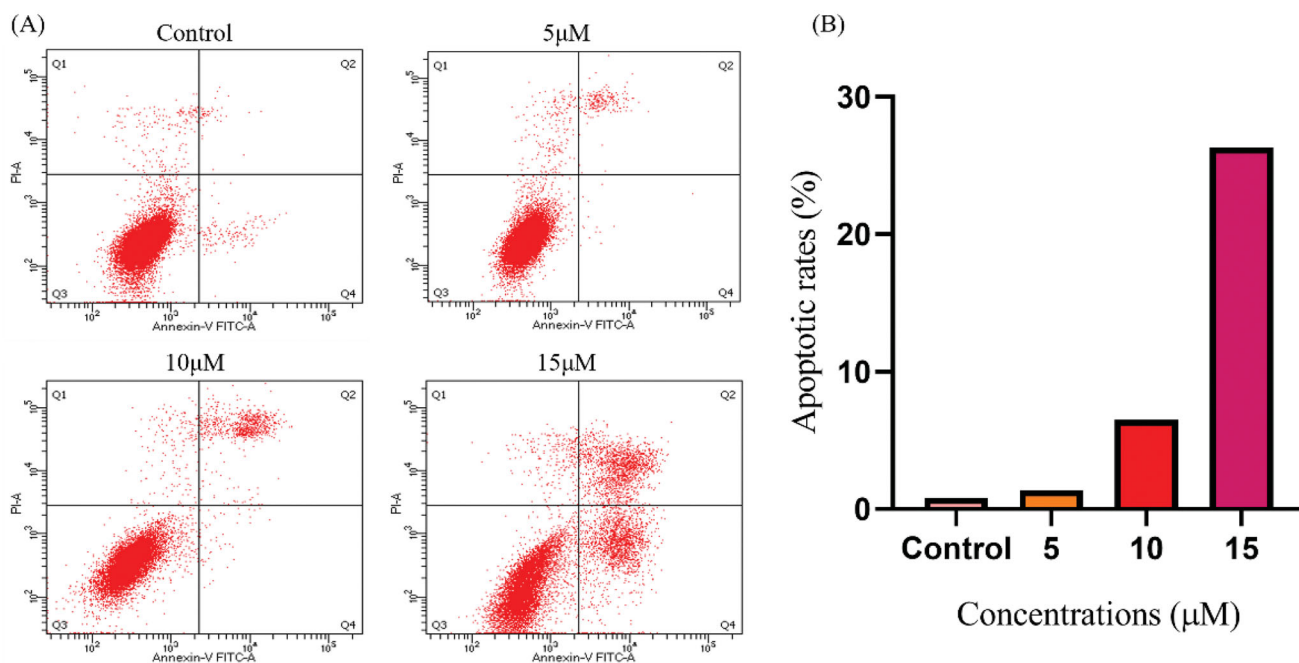
Figure 7. Compound **4k** induced A549 cells apoptosis. (A) A549 cells were treated with different concentrations of **4k** for 72 h and stained with PI/Annexin-V, and the apoptosis rates were determined by flow cytometry. (B) The histogram of apoptosis rates of A549 cells treated with various concentrations of **4k** (5 μM, 10 μM and 15 μM) for 72 h.

cells treated with different concentrations of compound **4k** were shown in Figure 3.

Inhibitory effect of 4k on intracellular tubulin polymerisation

In order to further confirm whether compound **4k** promotes or inhibits the formation of tubulin, purified porcine brain tubulin was cultured with compound **4k** (50 μM) and colchicine (6 μM), the reference control, respectively. Results revealed that **4k** was able to inhibit the polymerisation of tubulin, which was shown in Figure 4.

Immunofluorescence assay detected the effect of 4k on intracellular tubulin

In order to prove whether the compound **4k** targets microtubule to exert anti-tumour effects, an immunofluorescence assay had been taken to investigate whether **4k** could inhibit the disruption of microtubule in A549 cells (Figure 5). It could be observed that

the tubulin in control cells was evenly distributed throughout cells, maintaining the integrity of the cells. However, after being treated with different concentrations of **4k**, not only the structure of the cells change but also the intracellular microtubules began to aggregate around the nucleus. Furthermore, the cell structure was incomplete, and the tubulin distribution was diffuse, which could be further proved that **4k** exerts anti-tumour effects by acting on tubulin.

Effect of 4k on A549 cells migration

Aiming to investigate whether compound **4k** could inhibit the migration of A549 cells, the *in vitro* wound healing assay in A549 was performed (Figure 6). After being treated with different concentrations of **4k** for 24 h, it could be found that significant healing occurred in the control group, but the wound closure rates in the treatment groups were significantly lower than the control group. Besides, the histogram of wound closure rates revealed that with the increased concentration, the scratch healing rates
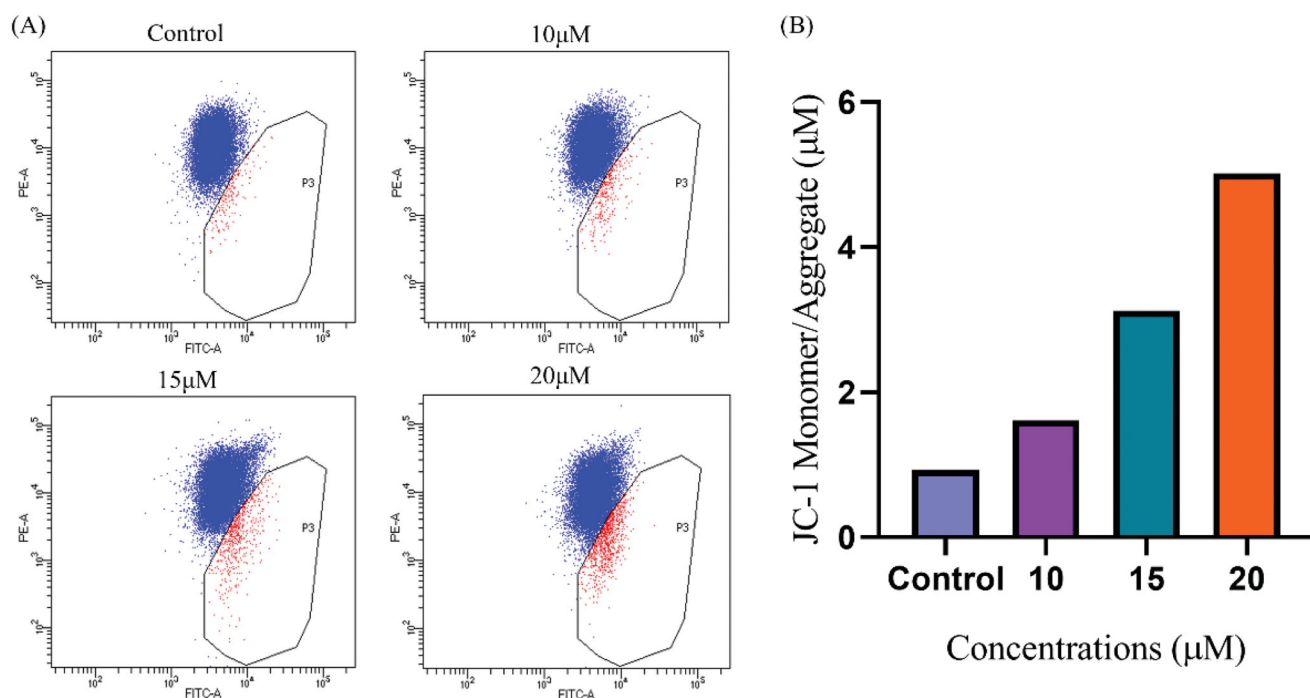
Figure 8. The effect of **4k** on mitochondrial membrane potential on A549 cells. (A) Analysis of mitochondrial membrane potential alterations by flow cytometry, and A549 cells were incubated with **4k** for 72 h before staining with JC-1. (B) The histogram of changes in mitochondrial membrane potential.
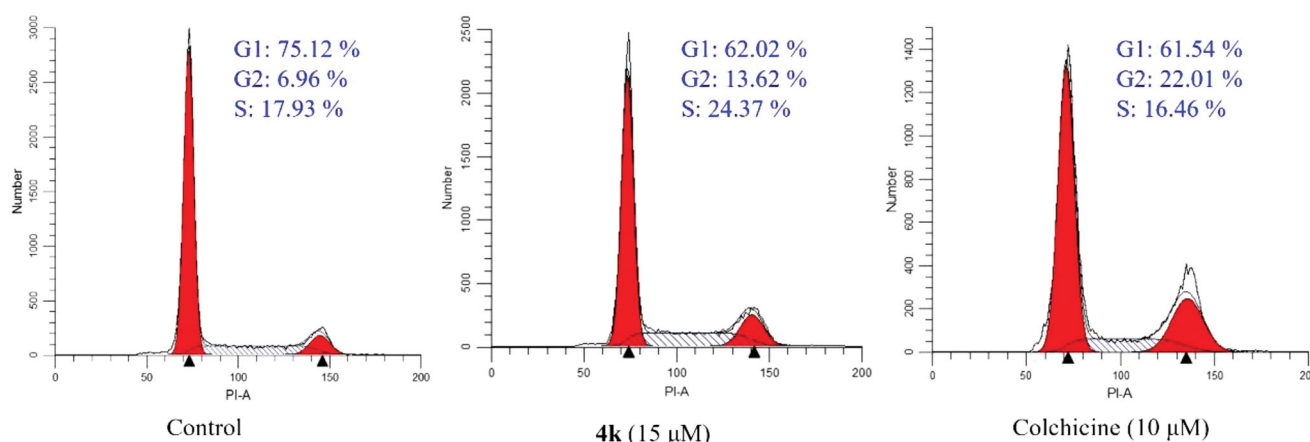
Figure 9. The analysis of cell cycle of A549 cells after treated with **4k** (15 μM) and colchicine (10 μM) for 72 h.

decreased significantly. All results displayed that **4k** could inhibit the migration of A549 in a dose-dependent manner obviously.

Effect of 4k on A549 cells apoptosis

In order to further verify whether **4k** induced apoptosis of A549 cells, the flow cytometry and PI/Annexin-V staining assays were used to detect the apoptosis of A549 cells under incubation with different concentrations of **4k** (Figure 7). The data showed that when A549 cells were incubated with **4k** for 72 h, with the increase of the concentration, the percentage of pro-apoptosis and late apoptosis increased significantly. Therefore, according to these results, it could be summarised that **4k** induced A549 cells apoptosis in a dose-dependent obviously.

Effects of 4k on mitochondrial membrane potential in A549 cells

The pathways that induce apoptosis are mediated by the death receptor pathway, mitochondrial pathway, endoplasmic reticulum stress pathway, and granzyme B pathway. It has been reported in the literature that microtubule-targeted inhibitors can induce apoptosis by relying on multiple pathways[29]. Therefore, the JC-1 method was carried out to test whether compound **4k** could induce a decrease in mitochondrial membrane potential. The experimental results displayed that with the increase of **4k** concentration (10 μM, 15 μM, 20 μM), the number of monomer components of JC-1 increased obviously (Figure 8), which proved **4k** could further induce apoptosis by reducing mitochondrial membrane potential.

Effects of 4k on cell cycle

The main mechanism for tubulin inhibitors to exert anti-tumour effects is to disrupt the homeostasis of tubulin by inhibiting or promoting tubulin polymerisation, while arresting the cell cycle at the G2/M phase, further inducing apoptosis of tumour cells[30]. Herein, the effect of **4k** on blocking the cell cycle was evaluated by flow

(A)

(B)

(C)

(D)
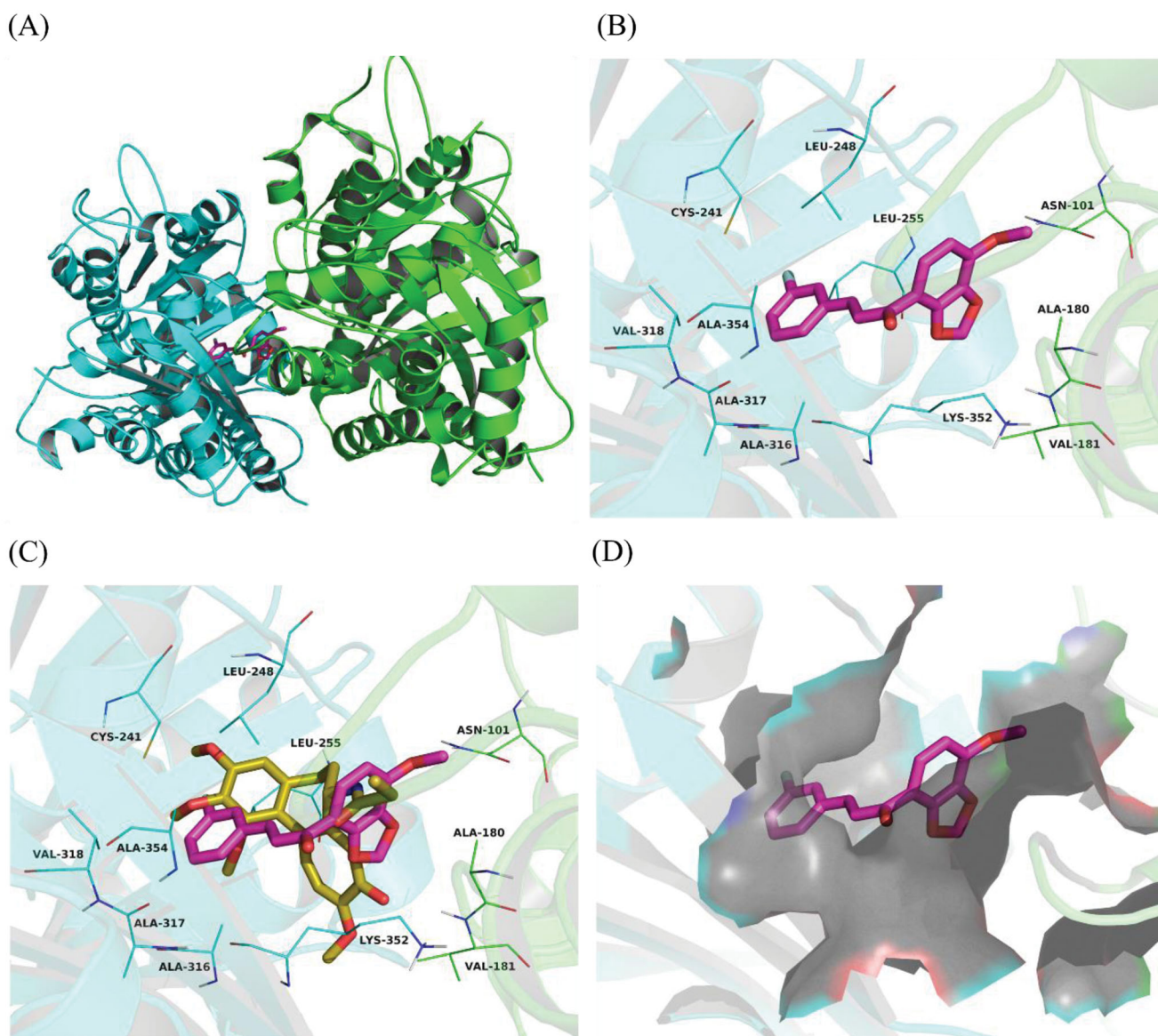
Figure 10. Compound **4k** was docked to the binding pocket of the α, β-tubulin (α: green; β: cyan). (A) Overall structure of α, β-tubulin with **4k**. (B) Binding pose of **4k** at colchicine binding site. (C) Superimposed pose of **4k** (rose red) and colchicine (yellow-orange) in the binding site. (D) Binding pose of **4k** in the surface of colchicine binding pocket.

cytometry. After treating with **4k** and colchicine at 15 μM or 10 μM for 72 h correspondingly, the proportion of cells in the G2/M phase of the cell cycle was 13.62% and 22.01%, respectively. While the ratio of A549 cells arrested in the G2/M phase of the control group was 6.96% (Figure 9). All results displayed that **4k** could block the cell cycle, which was similar to the reported literature[31].

Molecular Docking

Molecular docking studies had well clarified the binding mode of this series of synthetic compounds to the colchicine binding site of tubulin. Firstly, colchicine was docked with the colchicine site located on tubulin to verify whether the docking results were accurate. As shown in our previous report[32], the co-crystallized conformation of colchicine could be almost reproduced (RMSD: 1.083 Å), indicating that this molecular docking protocol could reproduce the crystalline form of colchicine. Then, molecular docking investigation between compound **4k** and tubulin crystal structure (PDB: 1SA0) was carried out. The results of docking

demonstrated that the estimated binding energy was −8.5 kcal•mol^{-1}. As depicted in Figure 10, **4k** was in an "L-shaped" conformation in the pocket of tubulin. Besides, **4k** located at the hydrophobic pocket of tubulin, which was surrounded by amino acid residues including Ala-180, Val-181, Leu-248, Leu-255, Ala-316, Val-317, Val-318, and Ala-354, forming a strong hydrophobic binding. The benzo[d][1,3]dioxole group of **4k** could form the cation-π interaction with Lys-352. These interactions contributed **4k** to anchor in the binding site of tubulin.

Conclusion

To sum up, a series of litseaone B derivatives were prepared as potential tubulin polymerizations and the bioactivities of inhibiting different cancer cell lines were also evaluated in our work. All results of investigations displayed that compound **4k** had excellent activity against cancer cells (A549, HepG2, HCT-15). Further research found that **4k** exerted anti-tumour effects on targeting tubulin and showed the inhibition of

tubulin polymerisation. Moreover, the wound healing assay revealed that compound **4k** could inhibit the migration of A549 cells in dose-dependent obviously. Additionally, results also displayed that **4k** could induce a decrease in the potential of the mitochondrial membrane, and further induce cell apoptosis. What's more, the cell cycle of A549 cells could be arrested at the G2/M phase as well. Collectively, all these results proved that **4k** had the potential to be developed and structurally modified as one kind of tubulin inhibitor in the future.

Disclosure statement

Funding

ORCID

Guangcheng Wang http://orcid.org/0000-0001-9104-337X

References

1. Jordan MA, Wilson L. Microtubules as a target for anticancer drugs. Nat Rev Cancer. 2004;4:253–65.
2. Kavallaris M. Microtubules and resistance to tubulin-binding agents. Nat Rev Cancer. 2010;10:194–204.
3. Nogales E. Structural insights into microtubule function. Ann Rev Biochem. 2000;69:277–302.
4. Jordan A, Hadfield JA, Lawrence NJ, McGown AT. Tubulin as a target for anticancer drugs: agents which interact with the mitotic spindle. Med Res Rev 1998;18:259–96.
5. Risinger AL, Giles FJ, Mooberry SL. Microtubule dynamics as a target in oncology. Cancer Treat Rev. 2009;35:255–61.
6. Bhalla KN. Microtubule-targeted anticancer agents and apoptosis. Oncogene. 2003;22:9075–86.
7. Dumontet C, Jordan MA. Microtubule-binding agents: a dynamic field of cancer therapeutics. Nat Rev Drug Discov. 2010;9:790–803.
8. Newman DJ, Cragg GM. Natural products as sources of new drugs from 1981 to 2014. J Nat Prod. 2016;79:629–61.
9. Yao H, Liu J, Xu S, Zhu Z, Xu J. The structural modification of natural products for novel drug discovery. Expert Opin Drug Discov. 2017;12:121–40.
10. Li G, Lou H-X. Strategies to diversify natural products for drug discovery. Med Res Rev. 2018;38:1255–94.
11. Thomford NE, Senthebane DA, Rowe A, Munro D, Seele P, Maroyi A, Dzobo K. Natural products for drug discovery in the 21st century: Innovations for novel drug discovery. Int J Mol Sci 2018;19(6):1578.
12. Haustedt LO, Mang C, Siems K, Schiewe H. Rational approaches to natural-product-based drug design. Curr Opin Drug Discov Devel. 2006;9:445–62.
13. Kingston DGI. Tubulin-interactive natural products as anti-cancer agents. J Nat Prod. 2009;72:507–15.
14. Yue Q-X, Liu X, Guo D-A. Microtubule-binding products for cancer therapy. Planta Med. 2010;76:1037–43.
15. Dall'Acqua S. Natural products as antimitotic agents. Curr Top Med Chem. 2014;14:2272–85.
16. Carlson RO. New tubulin targeting agents currently in clinical development. Expert Opin Investigat Drugs. 2008;17:707–22.
17. Wang Y-S, Wen Z-Q, Li B-T, Zhang H-B, Yang J-H. Ethnobotany, phytochemistry, and pharmacology of the genus litsea: an update. J Ethnopharmacol. 2016;181:66–107.
18. Jia X, Li P, Wan J, He C. A review on phytochemical and pharmacological properties of litsea coreana. Pharm Biol. 2017;55:1368–74.
19. Kong D-G, Zhao Y, Li G-H, et al. The genus litsea in traditional chinese medicine: an ethnomedical, phytochemical and pharmacological review. J Ethnopharmacol. 2015;164:256–64.
20. Li L, Zhao X, Luo Y, Zhao J, Yang X, Zhang H. Novel cytotoxic chalcones from litsea rubescens and litsea pedunculata. Bioorg Med Chem Lett. 2011;21:7431–3.
21. Sharma R, Kumar R, Kodwani R, Kapoor S, Khare A, Bansal R, Khurana S, Singh S, Thomas J, Roy B, et al. A review on mechanisms of anti tumor activity of chalcones. Anticancer Agents Med Chem. 2015;16:200–11.
22. Ducki S. Antimitotic chalcones and related compounds as inhibitors of tubulin assembly. Anticancer Agents Med Chem. 2009;9:336–47.
23. Lawrence NJ, McGown AT. The chemistry and biology of antimitotic chalcones and related enone systems. Curr Pharm Des. 2005;11:1679–93.
24. Mirzaei H, Shokrzadeh M, Modanloo M, Ziar A, Riazi GH, Emami S. New indole-based chalconoids as tubulin-targeting antiproliferative agentsd. Bioorg Chem. 2017;75:86–98.
25. Wang G, Li C, He L, Lei K, Wang F, Pu Y, Yang Z, Cao D, Ma L, Chen J. Design, synthesis and biological evaluation of a series of pyrano chalcone derivatives containing indole moiety as novel anti-tubulin agents. Bioorg Med Chem. 2014;22:2060–79.
26. Wang G, Qiu J, Chen M, Xiao X, Cao A, Li L. Synthesis, biological evaluation and docking studies of (e)-3-aryl-2-(3,4,5-trimethoxybenzoyl) acrylonitrile derivatives as anticancer agents. Latin Am J Pharmacy. 2017;36:1739–45.
27. Wang G, Peng Z, Zhang J, Qiu J, Xie Z, Gong Z. Synthesis, biological evaluation and molecular docking studies of aminochalcone derivatives as potential anticancer agents by targeting tubulin colchicine binding site. Bioorg Chem. 2018;78:332–40.
28. Wang G, Qiu J, Xiao X, Cao A, Zhou F. Synthesis, biological evaluation and molecular docking studies of a new series of chalcones containing naphthalene moiety as anticancer agents. Bioorg Chem. 2018;76:249–57.
29. Borowiak M, Nahaboo W, Reynders M, Nekolla K, Jalinot P, Hasserodt J, Rehberg M, Delattre M, Zahler S, Vollmar A, et al. Photoswitchable inhibitors of microtubule dynamics optically control mitosis and cell death. Cell. 2015;162:403–11.
30. Perez EA. Microtubule inhibitors: differentiating tubulin-inhibiting agents based on mechanisms of action, clinical activity, and resistance. Mol Cancer Ther. 2009;8:2086–95.
31. Sun M, Qin J, Kang Y, Zhang Y, Ba M, Yang H, Duan Y, Yao Y. 2-methoxydiol derivatives as new tubulin and HDAC dual-targeting inhibitors, displaying antitumor and antiangiogenic response. Bioorg Chem. 2022;120:105625.
32. Wang G, Liu W, Fan M, He M, Li Y, Peng Z. Design, synthesis and biological evaluation of novel thiazole-naphthalene derivatives as potential anticancer agents and tubulin polymerisation inhibitors. J Enzyme Inhib Med Chem. 2021;36:1694–702.